



Speckle Interferometry at SOAR in 2022

Brian D. Mason¹ , Andrei Tokovinin² , Rene A. Mendez³ , and Edgardo Costa³ ¹U.S. Naval Observatory, 3450 Massachusetts Ave., Washington, DC, USA; brian.d.mason.civ@us.navy.mil²Cerro Tololo Inter-American Observatory | NFFS NOIRLab Casilla 603, La Serena, Chile; andrei.tokovinin@noirlab.edu³Universidad de Chile, Casilla 36-D, Santiago, Chile; rmendez@uchile.cl

Received 2023 June 26; revised 2023 August 3; accepted 2023 August 4; published 2023 September 4

Abstract

Results of the speckle-interferometry observations at the 4.1 m SOuthern Astrophysical Research Telescope obtained during 2022 are presented: 2508 measurements of 1925 resolved pairs or subsystems and 785 nonresolutions of 611 targets; 26 pairs are resolved here for the first time. This work continues our long-term effort to monitor orbital motion in close binaries and hierarchical systems. A large number of orbits have been updated using these measurements.

Unified Astronomy Thesaurus concepts: [Interferometric binary stars \(806\)](#)

Supporting material: machine-readable tables

1. Introduction

This paper continues the series of double-star measurements made at the 4.1 m SOuthern Astrophysical Research Telescope (SOAR) since 2008 with the speckle interferometry detector package, high-resolution camera (HRCam). Previous results are published by Tokovinin et al. (2010a, hereafter [TMH10](#)) and in Tokovinin et al. (2010b, 2014, 2015, 2016, 2018, 2019, 2020, 2021, 2022), Hartkopf et al. (2012), and Tokovinin (2012). Observations reported here were made during 2022.

The structure and content of this paper are similar to other paper of this project. Section 2 reviews all speckle programs that contributed to this paper, the observing procedure and the data reduction. The results are presented in Section 3 in the form of electronic tables archived by the journal. We also discuss new resolutions and present orbits resulting from this data set. A short summary and an outlook of further work in Section 4 close the paper.

2. Observations

2.1. Observing Programs

As in previous years, HRCam (see Section 2.2) was used during 2022 to execute several observing programs, some with common targets. Table 1 gives an overview of these programs and indicates which observations are published in the present paper. The numbers of observations are approximate. Here is a brief description of the main programs.

Orbits of resolved binaries: new measurements contribute to the steady improvement of the quantity and quality of orbits in the Sixth Catalog of Orbits of Visual Binary Stars⁴ (Hartkopf et al. 2001). See Anguita-Aguero et al. (2022) and Gómez et al. (2022) as recent examples of this work. We provide large tables of reliable and preliminary orbits in Section 3.3.

Hierarchical systems of stars are of special interest because their architecture is relevant to star formation; dynamical evolution of these hierarchies increases chances of stellar interactions and mergers (Tokovinin 2021b). Orbital motions of several triple systems are monitored at SOAR and these data are used for the orbit determinations (Tokovinin & Latham 2020; Tokovinin 2021a, 2023).

Hipparcos binaries within 200 pc are monitored to measure masses of stars and to test stellar evolutionary models, as outlined by, e.g., Horch et al. (2015, 2017, 2019). The southern part of this sample is addressed at SOAR (Mendez et al. 2017). This program overlaps with the general work on visual orbits.

Neglected close binaries from the Washington Double Star Catalog (WDS; Mason et al. 2001),⁵ were observed as a “filler” at low priority. In some cases, we resolved new inner subsystems, thus converting classical visual pairs into hierarchical triples. In other cases we identified neglected pairs as spurious doubles in Section 3.4.

Nearby M dwarfs are being observed at SOAR since 2018 following the initiative of T. Henry and E. Vrijmoet. The goal is to assemble statistical data on orbital elements, focusing on short periods. First results on M dwarfs are published by Vrijmoet et al. (2022). In 2022, we continued to monitor these pairs; a paper on their orbits is in preparation. Measurements of previously known pairs are published here, those of newly resolved pairs are deferred to the paper in preparation.

TESS follow up continues the program executed in 2018–2020. Its results are published in Ziegler et al. (2020, 2021). All speckle observations of TESS targets of interest are promptly posted on the EXOFOP website⁶. These data are used in the growing number of papers on TESS exoplanets, mostly as limits on close companions to exohosts.

Acceleration stars were observed as potential targets of high-contrast imaging of exoplanets in a program led by K. Franson and B. Bowler (continued from 2021).

Gaia candidate hierarchies are wide binaries in the 100 pc catalog where one or both components have indications of unresolved subsystems in the Gaia data. A thousand of these

⁴ <https://crf.usno.navy.mil/wds-orb6/>

Original content from this work may be used under the terms of the [Creative Commons Attribution 4.0 licence](#). Any further distribution of this work must maintain attribution to the author(s) and the title of the work, journal citation and DOI.

⁵ See the latest online WDS version: <https://crf.usno.navy.mil/wds/>.

⁶ <https://exofop.ipac.caltech.edu/tess/>

Table 1
Observing Programs

Program	PI	<i>N</i>	Publ. ^a
Orbits, hierarchies	Mason, Tokovinin	1402	Yes
Hipparcos binaries	Mendez, Costa	247	Yes
Neglected binaries	R. Gould, Mason	390	Yes
Nearby M dwarfs	E. Vrijmoet	323	Some
TESS follow up	C. Ziegler	739	No
Acceleration stars	K. Franson	188	No
Gaia hierarchies	Tokovinin	1203	No
Wide pairs	J. Chanamé	275	No

Note.

^a This column indicates whether the results are published here (Yes), published partially (Some), or deferred to future papers (No).

candidates were observed during 2021–2023, about half were resolved, as reported in Tokovinin (2023).

Wide pairs were observed for the program led by J. Chanamé.

If observations of a given star were requested by several programs, they are published here even when the other program still continues. We also publish here the measurements of previously known pairs resolved during surveys, for example in the TESS follow up.

Speckle observations in 2022 were conducted during 13 observing runs for a total of approximately 18 nights (14 nights allocated and four nights of engineering time, usually second halves). A total of 5974 observations (including calibrators and reference stars) were made, 332 targets per night on average.

2.2. Instrument and Observing Procedure

The observations reported here were obtained with HRCam—a fast imager designed to work at the 4.1 m SOAR telescope (Tokovinin 2018). The instrument and observing procedure are described in the previous papers of these series (e.g., Tokovinin et al. 2020), so only the basic facts are restated here. HRCam receives light through the SOAR Adaptive Module, which provides correction of the atmospheric dispersion. We used mostly the near-infrared *I* filter (824 ± 170 nm) and the Strömgren *y* filter (543 ± 22 nm); the transmission curves of HRCam filters are given in the instrument manual⁷. In the standard observing mode, two series of $400 \times 200 \times 200$ pixel images (image cubes) are recorded. The pixel scale is $0''.01575$, so the field of view is $3''.15$; the exposure time is normally 24 ms. For survey programs such as TESS follow up, we use the *I* filter and a 2×2 binning, doubling the field. Pairs wider than $\sim 1''.4$ are observed with a 400×400 pixel field and the widest pairs are sometimes recorded with the full field of 1024 pixels ($16''$) and a 2×2 binning.

The speckle power spectra are calculated and displayed immediately after the acquisition for quick evaluation of the results. Observations of close pairs are accompanied by observations of single stars for reference to account for such instrumental effects as telescope vibration or aberrations. Bright stars can be resolved and measured below the formal diffraction limit by fitting a model to the power spectrum and using the reference. The resolution and contrast limits of HRCam are further discussed in TMH10 and in the previous

papers of this series. The standard magnitude limit is $I \approx 12$ mag under typical seeing; pairs as faint as $I \approx 16$ mag have been measured under exceptionally good seeing, albeit with reduced accuracy and resolution.

Custom software helps to optimize observations by selecting targets, pointing the telescope and logging. The observing programs are executed in an optimized way, depending on the target visibility, atmospheric conditions and priorities, while minimizing the telescope slews. Reference stars and calibrator binaries are observed alongside the main targets as needed; their observations are published here as well.

2.3. Data Processing

The data processing is described in TMH10 and Tokovinin (2018). We use the standard speckle-interferometry technique based on the calculation of the power spectrum and the speckle autocorrelation function (ACF). Companions are detected as secondary peaks in the ACF and/or as fringes in the power spectrum. Parameters of the binary and triple stars: separation (ρ), position angle (θ), and magnitude difference (Δm) are determined by modeling (fitting) the observed power spectrum. The true quadrant is found from the shift-and-add images whenever possible because the standard speckle interferometry determines position angles modulo 180° . The resolution and detection limits are estimated for each observation as described in TMH10.

Calibration of pixel scale and orientation is based on a set of wide pairs with well-modeled motion. The system of calibrators is tied to Gaia astrometry. Further details can be found in Tokovinin et al. (2022).

3. Results

3.1. Data Tables

The results (measures of resolved pairs and nonresolutions) are presented in exactly the same format as in Tokovinin et al. (2021, 2022). The long tables are published electronically; here we describe their content.

Table 2 lists 2508 measures of 1925 resolved pairs and subsystems, including new discoveries. The pairs are identified by their WDS-style codes based on the J2000 coordinates and discoverer designations adopted in the WDS catalog (Mason et al. 2001), as well as by alternative names in column (3), mostly from the Hipparcos catalog. Equatorial coordinates for the epoch J2000 in degrees are given in columns (4) and (5) to facilitate matching with other catalogs and databases. Circumstances of this particular observation (JY, filter, number of cubes), be it Tables 1 or 2, are given in columns (6) through (8). In the case of resolved multiple systems, the positional measurements and their errors (columns 9–12) and magnitude differences (column 13) refer to the individual pairings between components, not to their photocenters. As in the previous papers of this series, we list the internal errors derived from the power spectrum model and from the difference between the measures obtained from two data cubes. The real errors are usually larger, especially for difficult pairs with substantial Δm and/or with small separations. Residuals from orbits and from the models of calibrator binaries, typically between 1 and 5 mas rms, characterize the external errors of the HRCam astrometry.

The flags in column (14) indicate the cases where the true quadrant is determined (otherwise the position angle is measured modulo 180°), when the relative photometry of wide

⁷ <https://noirlab.edu/science/sites/default/files/media/archives/documents/scidoc1740.pdf>

Table 2
Measurements of Double Stars at SOAR

Col.	Label	Format	Description, units
1	WDS	A10	WDS code (J2000)
2	Discov.	A16	Discoverer code
3	Other	A12	Alternative name
4	R.A.	F8.4	R.A. J2000 (deg)
5	decl.	F8.4	decl. J2000 (deg)
6	Epoch	F9.4	Julian year (yr)
7	Filt.	A2	Filter
8	N	I2	Number of averaged cubes
9	θ	F8.1	Position angle (deg)
10	$\rho\sigma_\theta$	F5.1	Tangential error (mas)
11	ρ	F8.4	Separation (arcsec)
12	σ_ρ	F5.1	Radial error (mas)
13	Δm	F7.1	Magnitude difference (mag)
14	Flag	A1	Flag of magnitude difference ^a
15	$(O - C)_\theta$	F8.1	Residual in angle (deg)
16	$(O - C)_\rho$	F8.3	Residual in separation (arcsec)
17	Ref	A9	Orbit reference ^b

Notes.

^a Flags: q—the quadrant is determined; *— Δm and quadrant from average image; :—noisy data or tentative measures.

^b References are provided at https://crf.usno.navy.mil/data_products/WDS/orb6/wdsref.html.

(This table is available in its entirety in machine-readable form.)

pairs is derived from the long-exposure images (this reduces the bias caused by speckle anisoplanatism), and when the data are noisy or the resolutions are tentative (see [TMH10](#)). For binary stars with known orbits, the residuals to the latest orbit and its reference are provided in columns (15)–(17). Residuals close to 180° mean that the orbit swaps the brighter (A) and fainter (B) stars. However, in some binaries the secondary is fainter in one filter and brighter in the other (e.g., WDS15234–5919). In these cases, it is better to keep the historical identification of the components in agreement with the orbit and to provide a negative magnitude difference Δm .

The 785 nonresolutions of 611 systems are reported in Table 3. Its first columns (1) to (8) have the same meaning and format as in Table 2. Column (9) gives the minimum resolvable separation when pairs with $\Delta m < 1$ mag are detectable. It is computed from the maximum spatial frequency of the useful signal in the power spectrum and is normally close to the formal diffraction limit ($\frac{\lambda}{D}$). The following columns (10) and (11) provide the indicative dynamic range, i.e., the maximum magnitude difference at separations of $0''.15$ and $1''$, respectively, at 5σ detection level. The last column (12) marks noisy data by the flag “:.”

3.2. New Pairs

Table 4 highlights the 26 pairs resolved for the first time in 2022. All measurements of these pairs are found in Table 2. The pairs are identified by the WDS-style codes and the discovery codes or other names. The following columns contain the separation ρ , the magnitude difference Δm , and the observing program. About half of the new resolutions are Hipparcos stars within 200 pc with an increased Reduced Unit Weight Error (RUWE) in Gaia DR3 (GDR3; Gaia Collaboration et al. 2021). The second largest group are subsystems discovered in previously neglected visual binaries that lacked

Table 3
Unresolved Stars

Col.	Label	Format	Description, units
1	WDS	A10	WDS code (J2000)
2	Discov.	A16	Discoverer code
3	Other	A12	Alternative name
4	R.A.	F8.4	R.A. J2000 (deg)
5	decl.	F8.4	decl. J2000 (deg)
6	Epoch	F9.4	Julian year (yr)
7	Filt.	A2	Filter
8	N	I2	Number of averaged cubes
9	ρ_{\min}	F7.3	Angular resolution (arcsec)
10	$\Delta m(0.15)$	F7.2	Max. Δm at $0''.15$ (mag)
11	$\Delta m(1)$	F7.2	Max. Δm at $1''$ (mag)
12	Flag	A1	: marks noisy data

(This table is available in its entirety in machine-readable form.)

Table 4
New Double Stars

WDS J2000	Name	ρ (arcsec)	Δm (mag)	Program ^a
01079–4519	HIP5305	0.04	0.0	HIP ^b
01536–7018	HIP8834	0.29	1.6	HIP ^b
01575–5212	RST43Aa, Ab	0.08	1.4	MSC ^{c,d}
02469–6009	I268Ba, Bb	0.07	0.0	NEG ^{c,d}
05090+0654	HIP23961	1.84	2.0	HIP ^d
09275–7330	I832Aa, Ab	0.05	1.3	NEG ^c
09314–5724	RST3644Ba, Bb	0.06	0.4	NEG ^{c,d}
11093–1141	HIP54523	0.59	4.9	REF ^d
11260–5939	RST4476Aa, Ab	0.09	1.4	NEG ^{c,d}
11349–4908	HIP56497	1.14	5.7	REF ^d
12241+0357	LDS4205Ba, Bb	0.07	0.0	MSC
13133–0756	HDS1851Ba, Bb	0.04	0.5	NEG ^{c,d}
13557–3117	HIP68021	0.07	2.5	REF ^d
15531–1634	HDS2237Aa, Ab	0.04	1.4	NEG ^{c,d}
16000–2025	HLD125CD	0.41	0.0	MSC ^d
16161–3037	I1586Aa, Ab	0.04	1.6	ORB ^d
16580+0547	HD153252	0.37	1.0	MSC ^d
17323–4828	HIP85831	3.00	5.6	HIP ^d
17435–6856	HIP86741	0.44	2.8	HIP ^b
18274–3007	HIP90450	0.06	0.6	HIP ^{b,d}
20081–6745	HIP99174	0.12	0.7	HIP ^b
20372–6234	HIP101731	0.68	3.3	HIP ^b
20374–3444	HIP101752	0.05	0.3	HIP ^b
20581–1510	HIP103491	0.09	0.0	HIP ^b
21007–3518	BU765BC	0.07	2.4	NEG ^{c,d}
21046–5621	RST1081Aa, Ab	0.10	1.6	NEG ^{c,d}
21077–4523	HIP104296	0.03	0.0	HIP ^b
21232–1035	HIP105589	0.68	3.1	HIP ^b
23435–5947	HIP117033	0.24	2.4	HIP ^b

Notes.

^a HIP—Hipparcos suspected binary; MSC—multiple system; REF—reference star; NEG—neglected pair; ORB—orbit pair.

^b Suspected binary in Gaia DR3.

^c New subsystem in a neglected binary.

^d See comments in the text.

recent measures; six new triples are illustrated in Figure 1. Comments on some systems follow.

01575–5212. The newly resolved pair RST43Aa,Ab belongs to a quadruple system where the $0''.4$ pair RST 43BC is located at $3''.3$ from star A, a G6/K1III+F giant. The

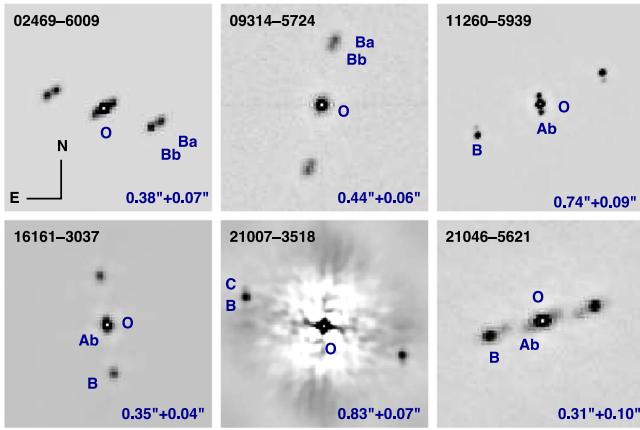


Figure 1. Fragments of speckle ACFs of six newly resolved triple stars. The spatial and intensity scale is chosen for best representation of each system. Blue letters mark the ACF peaks corresponding to the components’ location, O marks the ACF center. The outer and inner separations are indicated.

outer pair is COO10AB. The resolution of A is supported by its large RUWE = 20.2 in GDR3.

02469–6009 is a quadruple system where the new 0^{''}07 subsystem Ba,Bb has been discovered serendipitously in the 0^{''}4 visual pair I268AB. It has been observed at SOAR in 2016.96 without resolving the subsystem, owing to the lower quality of the power spectrum, while in 2022 the triple nature is clear (Figure 1). The outer component C of this system, at 20^{''}9, has common proper motion (PM) and parallax.

05090+0654. The newly resolved companion to HIP 23961 at 1^{''}84 is also found in GDR3 at a similar position of 144[°]16 and 1^{''}8250. Both stars have accurate and matching parallaxes of 13.4 mas and matching PMs, while $\Delta G = 2.36$ mag. However, between 2016.0 and 2022.2 the relative position has changed by 95 mas, which corresponds to a PM difference of 15 mas yr⁻¹. Meanwhile, Gaia measured a relative PM of only 2.1 mas yr⁻¹. Future observations will help to settle this discrepancy.

09314–5724 is another triple system discovered by resolving the secondary component of the neglected 0^{''}4 visual pair RST3644 with only three measures in the WDS. The resolution (Figure 1) is confirmed in 2023.

11093–1141. A new faint 0^{''}6 companion to the K5/M0III giant HIP 54523 (HD 96906), observed as a point-source reference, was resolved only in filter *y* and unresolved in *I*, where the magnitude difference should be larger because the main star is very red.

11260–5939. The neglected 0^{''}7 pair RST4476 contains a 0^{''}1 subsystem Aa,Ab (Figure 1). Very little information on this A2/2III star is available. Photometry suggests a distance of ~ 500 pc and no motion in the outer pair is detected since its discovery in 1939.

11349–4908. The new faint companion at 1^{''}14 from the bright reference star HIP 56497 with a fast PM of 250 mas yr⁻¹ could be optical.

13133–0756. The secondary star in the 0^{''}4 Hipparcos pair HDS1851 was resolved at a separation of 0^{''}04, slightly below the diffraction limit, so only elongation is seen. However, the discovery has been confirmed in 2023. The estimated period of Ba,Bb is about 25 yr.

13557–3117 A close 0^{''}07 companion to the reference star HIP 68021 (HD 121397, G6/8III) was discovered unexpectedly. However, it could have been suspected by the large

RUWE of 3.8 in GDR3 and by the acceleration reported by Brandt (2021).

15531–1634. Resolution of a 0^{''}04 subsystem Aa,Ab in the neglected Hipparcos binary HDS2237 (HD 142074, F6/7V) is tentative; in 2023.3 it was not detected, although the quality of the power spectrum was worse than in 2022.3. Reality of the subsystem is supported indirectly by the large RUWE of 15.9 in GDR3 and by the PM acceleration (Brandt 2021), which is unlikely to be produced by the outer 0^{''}4 pair A,B with an estimated period of ~ 300 yr.

16000–2025. This system, previously known as a visual triple HLD125 (AB at 2^{''}9 and AC at 27^{''}3), is converted into a quadruple by resolving star C into a 0^{''}4 equal pair. Star C was also seen double by Gaia: the DR3 catalog contains two nearly equal ($\Delta G = 0.10$ mag) sources at 0^{''}374 and 233[°]0 relative position. Our observation was prompted by Gaia, which should be credited for this discovery.

16161–3037 The visual pair I1568 was monitored by HRCam since 2008 to follow its slow orbit with $P = 160$ yr. Unexpectedly, the 0^{''}04 pair Aa,Ab was detected in 2022.44 and confirmed in 2023. Reexamination of the HRCam data shows that Aa,Ab was also resolved in 2018.23, but overlooked at the time, and partially resolved in 2022.68. Estimated period of Aa,Ab is 10 yr; it is responsible for the large astrometric noise in GDR3 (RUWE of 3.8). A wobble in the motion of AB caused by the subsystem could be detectable.

16580+0547 is a quadruple system HD 153252 (spectral type G0) of 3+1 hierarchy. The outer 60^{''} pair is CRV942 and its component A is a 5.52 days single-lined spectroscopic binary. Large astrometric noise of star A in GDR3 (RUWE of 8.6) suggested an intermediate subsystem Aa,Ab, which was indeed resolved at 0^{''}37. Its estimated period of ~ 400 yr implies only a slow motion, so the large RUWE could be produced by the companion’s light, rather than by the photocenter motion.

17323–4828. The faint companion found at 3^{''} from the high-PM star HIP 85831 is definitely optical. It is seen by Gaia DR3 at 1^{''}768 and 40[°]2 with $\Delta G = 4.9$ mag and a parallax of -0.06 mas.

18274–3007. Star HIP 90450 with a large RUWE of 5.0 has been resolved at 0^{''}06. A short period is expected and subsequent observations in 2022 and 2023 confirmed rapid retrograde motion of the new pair.

21007–3518. A new 0^{''}07 subsystem BC was resolved in a neglected 0^{''}7 visual binary BU765 (Figure 1). The estimated period of BC, ~ 10 yr, suggests rapid orbital motion.

21046–5621. A 0^{''}3 neglected pair RST1981 turns into a spectacular triple with inner 0^{''}1 pair Aa,Ab (Figure 1).

3.3. New and Updated Orbits

With one exception described below, the orbits here computed were determined with the venerable `orbgrid` code described in Hartkopf et al. (1989). In this technique, an adaptive “three-dimensional” grid search is performed for initial guesses of period P , epoch T and eccentricity e . Prior calculations of orbits for these pairs, as cited in Tables 5 and 6, provide good initial guesses of these elements. As the residuals are minimized, the grid spacing is reduced and this method continues until the grid steps fall below 0.01 yr in P and T and 0.001 in e . Measures with overly large residuals are given either lower or zero weight and the process repeats until the grid steps of 1% in magnitude of the prior iteration.

Table 5
Reliable Orbital Elements

WDS Desig. α, δ (2000)	Discoverer Designation	P (yr)	a ($''$)	i ($^\circ$)	Ω ($^\circ$)	T_0 (yr)	e	ω ($^\circ$)	Reference	Gr	Notes?
00160–4816	TOK808	6.98 ± 0.12	0.14759 ± 0.00063	23.0 ± 1.6	211.8 ± 5.8	2023.388 ± 0.024	0.3214 ± 0.0058	20.4 ± 8.7	Tok2023a	3	
00261–1123	YR4	39.12 0.75	0.2727 0.0026	150.3 5.2	81.0 8.7	2025.44 0.21	0.694 0.016	66. 11.	Tok2023a	3	
00324+0657	MCA1Aa, Ab	27.503 0.052	0.1594 0.0022	110.7 2.3	105.80 0.74	1989.00 0.10	0.810 0.024	14.4 2.2	Msn2021c	2	
01104–6727	GKI3	1.14451 0.00022	0.12478 0.00060	126.44 0.47	89.55 0.60	2013.4206 0.0057	0.1624 0.0030	39.3 2.1	Kpp2020f	1	
01388–1758	LDS838	26.351 0.049	2.0220 0.0042	128.78 0.52	146.22 0.43	2024.855 0.034	0.6143 0.0034	284.27 0.81	MnA2019	2	*
01559+0151	STF186	167.7 3.1	1.048 0.035	74.6 2.4	220.07 0.65	1893.8 3.1	0.717 0.057	44.3 3.5	Msn2021c	2	
02290–1959	RST2280Aa, Ab	31.50 0.49	0.5290 0.0070	163.5 1.7	168.3 5.2	2020.764 0.012	0.6497 0.0039	18.3 5.2	Tok2023a	3	
02418–5300	SYU4Ba, Bb	4.946 0.022	0.06887 0.00075	138.7 1.4	139.7 2.3	2021.179 0.019	0.4597 0.0093	276.0 3.0	Tok2023a	2	
02424+2001	BLA1Aa, Ab	8.868 0.016	0.05467 0.00067	71.50 0.62	101.07 0.75	1981.133 0.089	0.3767 0.0087	96.0 3.4	Msn1997a	1	
02434–6643	FIN333	35.19 0.16	0.269 0.010	92.20 0.78	33.99 0.24	1997.15 0.53	0.863 0.068	344.2 7.0	Msn2011a	3	
03125+1857	HDS408	9.525 0.058	0.0583 0.0020	121.3 9.6	155.0 4.9	2023.72 0.19	0.844 0.058	329. 10.	Cve2017b	3	
03271+1845	CHR10AB	8.408 0.025	0.0569 0.0018	25.7 9.0	190. 26.	2022.81 0.17	0.586 0.031	85. 31.	Tok2020e	2	
03311–0029	HDS444	20.41 0.90	0.0783 0.0020	37.1 3.1	49.6 7.6	2025.02 0.21	0.581 0.038	338. 11.	Tok2023a	3	
03544–4021	FIN344AB	14.077 0.015	0.06147 0.00027	31.50 0.88	65.5 1.8	2008.058 0.022	0.5847 0.0030	51.2 2.2	Tok2015c	2	
04108–4200	HDS530	23.80 0.74	0.224 0.013	110.6 2.5	193.0 1.6	2018.95 0.18	0.582 0.014	284.3 3.5	Tok2023a	3	
04119+2338	CHR14Aa, Ab	43.41 0.80	0.4200 0.0070	77.5 3.1	156.1 1.6	1993.31 0.39	0.924 0.028	258.7 7.7	Msn2010a	3	
04312+0157	HDS585	74.78 0.28	0.3941 0.0020	76.68 0.15	80.40 0.25	2013.975 0.069	0.4705 0.0023	346.33 0.46	Tok2019c	3	
04330–1633	CRI7Ba, Bb	5.685 0.039	0.0887 0.0018	98.48 0.45	171.07 0.90	2017.39 0.17	0.1969 0.0057	77.4 9.2	Tok2023a	3	
04400–3105	HDS602	28.01 0.20	0.3112 0.0019	118.10 0.40	174.47 0.40	2021.796 0.019	0.6963 0.0015	81.51 0.92	Tok2019c	3	
04590–1623	BU314AB	54.98 0.10	0.4783 0.0042	119.0 4.2	129.20 0.61	2033.84 0.12	0.927 0.017	334.7 1.3	Doc2019e	2	
05174–3522	TSN1	0.71094 0.00038	0.05853 0.00042	107.94 0.39	164.26 0.55	2022.3670 0.0056	0.2242 0.0041	140.7 3.0	Tok2023a	2	

Table 5
(Continued)

WDS Desig. α, δ (2000)	Discoverer Designation	P (yr)	a ($''$)	i ($^\circ$)	Ω ($^\circ$)	T_0 (yr)	e	ω ($^\circ$)	Reference	Gr	Notes?
05429–0648	A494AB	20.1843 0.0062	0.20976 0.00072	72.15 0.11	96.52 0.18	1959.954 0.028	0.39553 0.00097	273.97 0.45	Msn2009	2	
05525–0217	HDS787	11.851 0.023	0.1200 0.0015	56.90 0.66	153.3 1.1	1999.917 0.067	0.2285 0.0034	91.8 2.5	Tok2017b	2	
06035+1941	MCA24	13.021 0.029	0.0512 0.0016	111.4 6.3	227.4 2.5	2006.64 0.11	0.806 0.045	296.6 6.9	Tok2020e	2	
06159+0110	RST5225	29.551 0.037	0.16583 0.00078	13.7 1.9	185.6 9.9	1995.128 0.060	0.3773 0.0035	197. 10.	Msn2009	2	
06214+0216	A2667	96.5 1.7	0.4243 0.0018	62.85 0.47	110.30 0.20	1933.1 1.8	0.4225 0.0047	252.0 2.1	Msn2009	2	
06237–3319	TOK823Aa, Ab	5.013 0.031	0.04626 0.00028	129.9 1.3	199.4 1.0	2022.060 0.013	0.6601 0.0081	327.3 1.8	Tok2022g	3	
06510+0551	HDS950	29.11 0.23	0.1205 0.0047	98.02 0.68	162.3 1.3	2016.79 0.36	0.3977 0.0050	270.7 5.4	Tok2019c	3	
07043–0303	A519AB	43.84 0.34	0.2765 0.0025	98.85 0.44	96.28 0.12	2007.446 0.093	0.559 0.011	0.49 0.75	Tok2015c	2	
07508+0317	A2880	109.6 2.1	0.1815 0.0022	47.86 0.45	93.32 0.57	1991.903 0.065	0.6046 0.0055	291.23 0.66	Hrt2000a	2	
07548–6613	TOK830	7.46 0.15	0.05329 0.00097	147.9 1.5	114.8 2.9	2021.638 0.016	0.4088 0.0099	98.6 3.1	Tok2022g	3	
08280–3507	FIN314Aa, Ab	35.41 0.19	0.07833 0.00046	38.8 4.8	289. 12.	2005.25 0.39	0.9279 0.0090	297. 16.	Tok2018e	3	
08539+0149	A2554	44.43 0.19	0.2102 0.0011	161.4 2.1	311.8 5.8	2021.750 0.064	0.4859 0.0053	0.8 6.3	Tok2015c	2	
08589+0829	DEL2	5.5340 0.0036	0.3925 0.0019	123.1 1.2	279.89 0.60	2006.434 0.39	0.7723 0.0082	19.9 1.2	Tok2015c	2	
09125–4032	B1115	135.49 0.60	0.33052 0.00072	141.98 0.16	104.37 0.47	2005.782 0.025	0.4413 0.0018	271.57 0.36	Tok2014a	3	
09156–1036	MTG2	5.0419 0.0023	0.1992 0.0010	116.23 0.59	112.81 0.52	2014.191 0.015	0.4760 0.0045	273.0 1.3	Msn2021a	2	
09243–3926	FIN348	41.58 0.19	0.12249 0.00047	160.5 2.1	91.3 2.7	2004.920 0.095	0.4589 0.0065	336.0 3.0	Tok2021f	2	
09307–4028	COP1	34.11 0.12	0.8110 0.0017	58.45 0.15	288.24 0.13	2004.062 0.035	0.4375 0.0030	47.76 0.53	Msn2021a	1	
09442–2746	FIN326	18.423 0.019	0.10904 0.00032	126.19 0.44	175.66 0.44	2020.913 0.025	0.4956 0.0031	138.04 0.86	Tok2020e	1	
10112–3245	HDS1469	18.68 1.04	0.1076 0.0069	121.6 2.4	255.2 3.8	2018.22 0.15	0.407 0.030	343.8 4.1	Tok2016e	3	*
10214–2616	HDS1491	22.14 0.28	0.11934 0.00038	150.1 1.0	250.79 0.92	2024.09 0.11	0.1954 0.0036	1.1 3.5	Tok2019c	3	
10282–2548	FIN308AB	32.57 0.11	0.1442 0.0019	48.2 1.2	157.8 1.9	2018.157 0.076	0.7375 0.0051	269.3 2.8	Tok2015c	2	

Table 5
(Continued)

WDS Desig. α, δ (2000)	Discoverer Designation	P (yr)	a ($''$)	i ($^\circ$)	Ω ($^\circ$)	T_0 (yr)	e	ω ($^\circ$)	Reference	Gr	Notes?
10430–0913	WSI112	27.62 0.24	0.577 0.012	121.0 2.7	282.6 1.1	2002.11 0.11	0.440 0.024	284.1 3.1	Tok2022g	3	
11272–1539	HU462	48.16 0.75	0.4579 0.0056	169.0 4.9	135. 18.	1960.9 1.1	0.091 0.012	1. 14.	Msn2021c	2	
11436–1401	YSC210	17.899 0.031	0.16328 0.00034	117.81 0.14	207.83 0.23	2008.808 0.056	0.1684 0.0017	134.9 1.2	Tok2023a	3	
12290+0826	WSI113	11.6373 0.0052	0.3088 0.0016	108.43 0.14	188.87 0.35	2008.206 0.022	0.29482 0.00077	89.00 0.79	AST2016	2	
13123–5955	SEE170AB	27.51 0.42	0.16644 0.00093	60.22 0.96	279.8 1.0	2022.140 0.071	0.6657 0.0084	18.3 2.8	Doc2021d	2	
13217–3919	HDS1875	40.72 0.77	0.2024 0.0031	119.83 0.66	195.1 1.7	2019.518 0.091	0.5250 0.0062	230.73 0.94	Tok2020g	3	
13574–6229	FIN370	18.757 0.017	0.13544 0.00026	144.34 0.33	269.32 0.48	2005.849 0.023	0.2193 0.0020	359.81 0.77	Mdz2021	2	
14275–3527	TOK724	4.103 0.020	0.0381 0.0011	89.40 0.67	317.62 0.60	2018.499 0.054	0.480 0.037	31.3 5.1	Tok2022g	2	
14462–2111	FIN309	12.9212 0.0065	0.18189 0.00051	28.24 0.74	287.0 2.0	1995.265 0.019	0.6373 0.0022	34.6 2.4	Msn2010c	1	
14567–6247	FIN372	38.20 0.20	0.08808 0.00073	146.8 1.8	223.8 3.0	1993.76 0.24	0.2775 0.0080	64.7 4.9	Msn2010c	2	
14589+0636	WSI81	5.4589 0.0052	0.09533 0.00041	154.3 1.1	44.7 2.7	2016.653 0.012	0.4059 0.0030	328.5 3.2	Tok2018e	2	
15122–1948	B2351Aa, Ab	23.512 0.026	0.12932 0.00064	154.2 1.0	173.8 2.3	1971.034 0.076	0.2440 0.0029	340.1 2.8	Msn2021c	1	
15537–0429	TOK725	11.26 0.13	0.08241 0.00064	166.6 4.5	198. 20.	2020.729 0.027	0.5685 0.0081	334. 20.	Tok2021f	3	
16430–0857	YSC155	10.772 0.081	0.0655 0.0011	118.0 3.4	149.1 2.1	2021.631 0.087	0.738 0.029	12.8 5.2	Tok2021f	2	
16555–0820	KUI75AB	1.71741 0.00005	0.22949 0.00046	161.30 0.49	164.7 1.6	1991.6311 0.0063	0.04225 0.00092	128.7 2.3	Sod1999	1	*
17077+0722	YSC62	14.327 0.025	0.30649 0.00094	113.09 0.34	241.44 0.27	2006.535 0.028	0.4889 0.0034	23.57 0.79	Mdz2021	2	
17119–0151	LPM629	34.484 0.029	0.7688 0.0021	19.94 0.88	143.9 4.4	1988.130 0.057	0.1969 0.0034	218.7 4.6	Doc2018l	3	
17151–2750	ELP40	19.789 0.086	0.11741 0.00084	141.8 1.6	39.4 1.4	2009.20 0.12	0.2392 0.0084	11.8 3.3	Tok2022g	3	
17190–3459	MLO4AB	42.152 0.039	1.8260 0.0017	127.662 0.034	133.574 0.063	1933.752 0.079	0.57374 0.00029	68.451 0.056	Izm2019	1	*
17304–0104	STF2173AB	46.585 0.023	0.96971 0.00060	99.177 0.037	151.769 0.033	2008.601 0.037	0.17636 0.00074	324.57 0.32	Hei1994a	1	*
19167–4553	RST4036	7.6834 0.0052	0.24586 0.00018	124.499 0.066	200.172 0.097	1995.043 0.016	0.26067 0.00064	240.72 0.24	Msn2019	1	

Table 5
(Continued)

WDS Desig. α, δ (2000)	Discoverer Designation	P (yr)	a (")	i ($^{\circ}$)	Ω ($^{\circ}$)	T_0 (yr)	e	ω ($^{\circ}$)	Reference	Gr	Notes?
21044–1951	FIN328	27.896 0.032	0.2639 0.0016	163.7 3.4	160.4 9.8	2002.41 0.13	0.4087 0.0068	47. 11.	Doc2013d	2	
21214+1020	A617	6.0570 0.0019	0.0969 0.0011	132.4 4.4	281.1 2.1	1991.855 0.023	0.827 0.020	13.2 3.3	Sod1999	1	
21274–0701	HDS3053	20.633 0.051	0.16476 0.00066	50.27 0.40	152.93 0.52	2015.756 0.044	0.3545 0.0027	149.3 1.1	Mit2021	2	
22508–6543	HDS3246	20.390 0.070	0.2110 0.0011	94.01 0.15	92.50 0.20	2016.327 0.054	0.4202 0.0019	326.1 1.3	Tok2018e	3	
22532–3750	HDS3250Aa, Ab	12.91 0.47	0.1261 0.0048	42.5 3.0	42.5 4.8	2012.00 0.48	0.086 0.030	322. 18.	Tok2020e	3	
23191–1328	MCA74Aa, Ab	6.3211 0.0041	0.1912 0.0023	46.8 1.2	158.7 1.8	2012.405 0.058	0.1735 0.0062	37.1 4.3	Doc2018f	1	

Individual measures are weighted according to the methodology described in Section 2.1 of Hartkopf et al. (2001). This determines the weight of each observation based on N , the number of nights (often one) in a mean position, the observation technique, and a factor which takes into account the measured separation and the resolution capability of the telescope at the wavelength used for the observation.

Again, using the algorithm outlined in Hartkopf et al. (2001) the numerical “grade” is given to each calculated orbit. The subjective qualification of these numerical grades are: 1 = definitive, 2 = good, 3 = reliable, 4 = preliminary, and 5 = indeterminate. The actual grading is done with an objective rubric evaluating each orbit by several criteria:

1. weighted rms residual in separation ($d\rho$);
2. weighted rms residual in relative separation ($\frac{d\rho}{\rho}$);
3. position angle (θ) coverage (most helpful evaluating high eccentricity orbits);
4. maximum gap in position angle coverage (θ);
5. phase coverage, calculated from P and T (most helpful evaluating high inclination orbits);
6. maximum gap in phase;
7. number of revolutions; and
8. total number of observations.

The final list of computed orbits are divided into two groups: reliable and preliminary. However, rather than basing this solely on the grade the criterion of Aitken (1964) is applied:

“In general, it is not worth while to compute the orbit of a double star until the observed arc not only exceeds 180° , but also defines both ends of the apparent ellipse.”

The orbits meeting this criteria and having small ($\frac{\Delta P}{P}$) relative error are found in the table of reliable orbits and other orbit solutions are in the table of preliminary orbits. While these preliminary orbits may lack sufficient coverage at this time, they should allow the determination of accurate predicted

positions for the next years. Some of these orbits were improved with the addition of data taken in the first half of 2023, which will be presented with the rest of the SOAR 2023 data next year.

In these tables, the system is identified by the WDS J2000 code and the Discoverer Designation, followed by the seven Campbell Elements. Following this, a reference to the most current Hartkopf et al. (2001) orbit, which has been here improved, is given. This is followed by the orbit grade and a flag indicating if there is a note. In Table 5, the following line provides the error of each orbital element. The quoted precision of each element is determined from the precision of the error, which is given to two significant digits. In Table 6, errors are not provided, but the elements are given to the nearest degree for i , Ω and ω , to nearest tenth of a year for P and T and the to a tenth of a percent for a and e . If a higher precision is provided in Table 6, this is due to the precision of the error in that element.

Notes to individual systems in both tables follow.

3.3.1. Notes to Individual Orbital Systems

01388–1758 = LDS838 : Using the parallax from GDR3 and the mass ratio from Worley & Behall (1973), individual masses of $\mathcal{M}_a = 0.1191 \pm 0.0018 \mathcal{M}_{\odot}$ and $\mathcal{M}_b = 0.1144 \pm 0.0017 \mathcal{M}_{\odot}$ are determined for these components. See Figure 2.

10112–3245 = HDS1469: radically different solution for this pair. See Figure 2.

13535+1257 = BEU18: this pair lacks data in the south to define that portion of the orbit. Data in Autumn 2023 or Spring 2031 would characterize those parts of the orbit.

14516–4335 = FIN319: this pair lacks data when the secondary is east of the primary. However, the separation predicted here ($0''.017$) would be a challenge. Close to this may be the best we can do. It is predicted to move from $343^{\circ}0$ & $0''.042$ on 2031.0 counterclockwise to $214^{\circ}4$ & $0''.047$ on 2032.0. Observing the pair many times in 2031 will be key to improving this orbit.

15440+0231 = RDR6Ba,Bb: predicted to get as close as $0''.007$ at periastron, observing “both ends of the apparent ellipse” will be challenging. However, measures approaching

Table 6
Provisional Orbital Elements

WDS Desig. α, δ (2000)	Discoverer Designation	P (yr)	a ($''$)	i ($^\circ$)	Ω ($^\circ$)	T_0 (yr)	e	ω ($^\circ$)	Reference	Gr	Notes?
00003–4417	I1477	119.1	0.424	60.8	148.7	2012.9	0.710	299.	Cve2010e	3	
00164–7024	HEI198	52.4	0.1122	144.9	176.3	2012.33	0.483	238.	Tok2017b	3	
02514–2139	DON43	121.2	0.2068	41.5	209.	1976.0	0.399	283.	Doc2016i	3	
03526–0829	RST4762AB	151.4	0.1668	120.1	264.8	1994.0	0.264	327.	Tok2023a	3	
05033–2315	BEU7	15.34	0.326	136.3	273.	2022.2	0.093	75.	Tok2023a	4	
05320–0018	HEI42Aa, Ab	317.4	0.355	107.3	142.8	1960.2	0.6750	257.	Tok2014a	4	
06337–2853	B700	200.5	0.219	114.7	145.9	2008.7	0.826	133.	Tok2023a	4	
06354–0403	JNN271	10.4	0.2017	88.42	171.47	2022.6	0.263	9.	Tok2023a	4	
07175–4659	I7	85.9	1.05	104.	242.2	1958.4	0.976	251.	Tok2015c	3	
07185–5721	HDS1013Aa, Ab	56.6	0.3511	20.	171.	1997.9	0.216	124.	Hrt2012a	3	
07417+0942	STF1130	902.9	1.776	51.7	327.6	1981.2	0.793	346.5	Msn1999a	4	
07522–4035	TOK195	7.149	0.0611	82.9	272.24	2012.13	0.385	350.	Tok2015c	3	
08085–5237	B1586	201.8	0.314	74.42	86.1	2018.94	0.8476	297.0	Tok2022g	4	
08369–7857	KOH79AB	56.2	0.1953	108.5	181.17	1991.6	0.1786	279.	Tok2016e	3	
08486+0237	A2551	73.7	0.1484	36.8	160.2	1951.1	0.663	70.	Msn2017g	3	
10283–2416	TOK537Aa, Ab	31.2	0.336	55.11	157.10	2021.825	0.694	10.7	Tok2021f	4	
10595–4130	RST2720	217.2	0.210	31.	241.	1975.4	0.241	53.	Tok2023a	4	
11128–7402	B2009	142.0	0.276	140.	290.	1971.4	0.241	295.	Tok2023a	4	
11192–1950	TOK383Aa, Ab	12.67	0.0429	134.9	177.0	2020.09	0.380	328.	Tok2020g	3	
11431–3601	I1546	149.6	0.2017	121.3	272.9	2000.6	0.137	286.	Tok2022g	4	
12096–6727	HDS1716	56.2	0.150	53.6	57.6	2019.08	0.503	351.2	Tok2019c	3	
12117–5222	RIZ2	3.626	0.0440	164.	225.	2019.237	0.619	54.	Tok2023a	3	
12228–0405	BWL29AB	9.783	0.234	103.8	210.2	2023.56	0.741	252.	Tok2023a	4	
12446–5717	FIN65AB	111.6	0.292	112.1	242.7	1946.1	0.413	114.	Doc2013d	3	
13344–5931	TOK403	17.03	0.1423	117.53	252.65	2021.090	0.4587	90.3	Tok2020e	3	
13535+1257	BEU18	7.4020	0.18275	127.31	187.62	2023.701	0.5207	355.5	Tok2022g	2	*
14516–4335	FIN319	10.874	0.0853	30.8	118.0	2020.650	0.8013	344.2	Doc2020d	2	*
15251–2340	RST2957	57.21	0.21689	85.59	93.019	2027.57	0.5505	338.4	Tok2016e	3	
15273+0942	A1120	51.8	0.174	67.0	156.2	1931.4	0.723	340.	Msn2014b	3	
15394–1355	HDS2210	41.12	0.1701	109.4	172.34	2014.8	0.054	11.	Tok2018e	3	
15433–0515	TOK594Aa, Ab	3.809	0.0561	57.5	142.2	2019.053	0.791	137.2	Tok2021f	3	
15440+0231	RDR6Ba, Bb	2.9726	0.1267	126.	190.5	2022.868	0.939	331.7	Tok2021b	2	*
15462–2804	KOH49Ca, Cb	18.811	0.11663	136.55	280.7	2038.514	0.3114	35.54	Tok2021c	2	*
16016–7843	HDS2259	62.9	0.361	88.2	156.46	2004.30	0.801	45.	Tok2023a	4	
16038+1406	HDS2265	50.2	0.335	59.0	178.1	2021.16	0.840	343.	Tok2020e	4	
16271–1205	HU158	234.3	0.297	107.9	315.1	2000.1	0.682	358.2	Tok2022g	4	
16514–2450	B2397	69.6	0.1578	119.0	201.2	2020.4	0.067	250.	Tok2019c	3	
16573–5344	SYU11Aa, Ab	9.104	0.08702	6.6	174.	2023.934	0.5708	333.	Tok2022g	3	
17207–0706	A2593AB	75.5	0.2589	128.9	167.6	1986.9	0.094	48.	Msn2014a	3	
17375–3747	B915AB	128.4	0.278	65.2	314.2	2147.0	0.052	25.	Msn2017a	4	
17387–2155	HDS2492	21.48	0.1027	26.9	220.	2006.47	0.392	15.	Tok2023a	3	
17460–3435	HDS2510AB	41.5	0.134	64.3	241.4	2012.1	0.298	304.	Tok2022g	3	
18281–2645	HDS2615AB	37.29	0.557	95.6	173.23	1988.66	0.794	84.5	Tok2015c	3	
19474–0148	A2993AB	64.1	0.1396	130.1	174.4	2026.92	0.6880	46.0	Hrt2014b	3	
20073–5127	RST1059	161.7	0.1697	17.8	259.	2014.5	0.275	315.	Mdz2017	3	
23209+1643	HEI88	34.09	0.16872	25.2	120.2	2002.97	0.6365	268.1	Cve2011a	3	
23218–1217	HU95	162.2	0.3994	155.	202.	1943.2	0.374	113.	Msn1999c	4	
23286–3821	HDS3342	47.7	0.1175	129.5	305.7	2014.9	0.359	337.1	Tok2019c	3	
23455–1610	MTG5	21.46	0.4192	98.65	9.13	2024.373	0.4761	352.7	Tok2023a	3	

and coming out of periastron as well as nondetection (see Table 3) when predicted should adequately probe this in Autumn 2025.

15462–2804 = KOH49Ca,Cb: this pair just needs more data to adequately define the eastern end of the apparent ellipse. It should get to widest separation by mid 2027 and begin closing at that time.

16555–0820 = KUI75AB: using parallax from van Leeuwen (2007) and the mass ratio from Harris et al. (1963), individual masses of $\mathcal{M}_a = 0.487 \pm 0.054 \mathcal{M}_\odot$ and $\mathcal{M}_b = 0.487 \pm 0.054 \mathcal{M}_\odot$ are determined for these components. See Figure 2.

17190–3459 = MLO4AB: using parallax from van Leeuwen (2007) and the mass ratio from Harris et al. (1963), individual masses of $\mathcal{M}_a = 0.65 \pm 0.12 \mathcal{M}_\odot$ and $\mathcal{M}_b = 0.448 \pm 0.085 \mathcal{M}_\odot$ are determined for these components. See Figure 2.

17304–0104 = STF2173AB: the program `orbgrid` was used here to identify measures having overly large residuals which were omitted from the solution. High-angular resolution measures only (speckle interferometry, adaptive optics, Hipparcos, phase grating interferometer) were coupled with radial velocities from Batten et al. (1991) and Duquennoy et al. (1991), to arrive at a combined solution using the `orbit IDL`

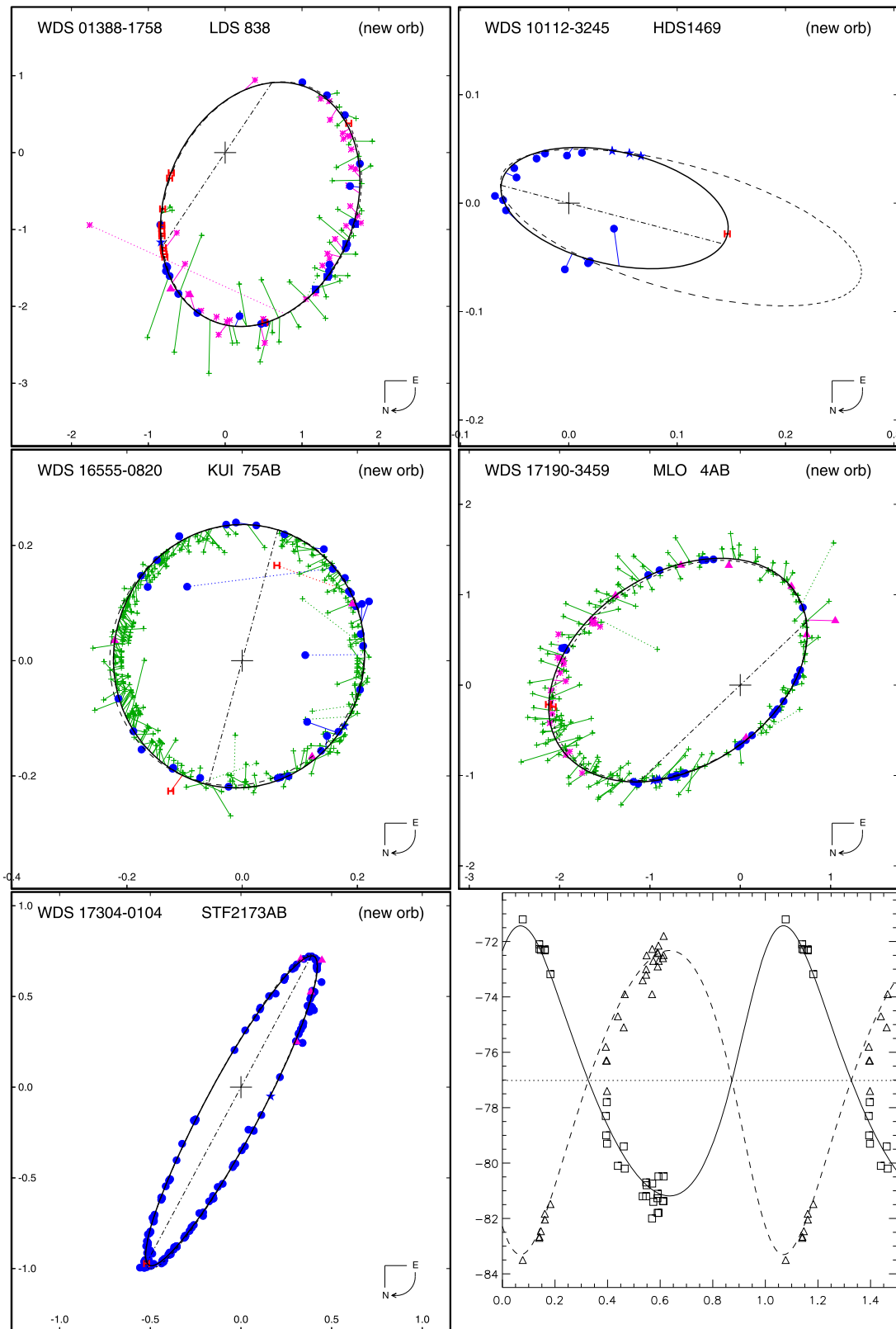


Figure 2. Selected new orbital solutions, plotted together with all published data in the WDS database as well as the new data in Table 2. In each of these figures, micrometric observations are indicated by plus signs, interferometric measures by filled circles, conventional CCD by pink triangles, space-based measures are indicated by the letter “H,” new measures from Table 2 are plotted as a filled star. “O–C” lines connect each measure to its predicted position along the new orbit (shown as a thick solid line). A dotted–dashed line indicates the line of nodes, and a curved arrow in the lower right corner of each figure indicates the direction of orbital motion. The earlier orbit referenced in Table 5 is shown as a dashed ellipse. For the combined orbit of 17304–0104 = STF2173, plots of the relative astrometry and the radial velocity curve are provided.

code Tokovinin (2016b), resulting in additional orbital elements of $K_1 = 5.00 \pm 0.11 \text{ km s}^{-1}$, $K_2 = 5.40 \pm 0.11 \text{ km s}^{-1}$, $\gamma = -77.197 \pm 0.064 \text{ km s}^{-1}$, and individual masses of $\mathcal{M}_a = 1.018 \pm 0.048 \mathcal{M}_\odot$ and $\mathcal{M}_b = 0.943 \pm 0.046 \mathcal{M}_\odot$ are determined for these components. In addition, an orbital parallax of $59.84 \pm 2.89 \text{ mas}$ is determined, which compares quite well with the mean trigonometric parallax of 59.6071 mas from the Gaia Collaboration et al. (2018). See Figure 2.

3.4. Spurious Pairs

False detections of double stars can be caused by errors in pointing, in data processing, or by other reasons; see Table 5 and Section 4 of McAlister et al. (1993). Optical artifacts resembling binary companions are discussed in Tokovinin et al. (2010a) and Tokovinin (2018). Identifying these spurious pairs will save observing time in the future by eliminating the need to follow up and examine these targets. In Table 7 are listed pairs we consider as likely spurious. The table contains the WDS code and Discoverer designation, the method (Vis—visual micrometer, Sp—speckle, HIP—Hipparcos) and date of the original discovery and the year(s) it has been unresolved in this program. Following that is a code giving other indications supporting the characterization of the double as “spurious.” These codes are: R—normal RUWE parameter in GDR3, hence lack of astrometric noise; L—long estimated period, making it unlikely that the pair has moved significantly between discovery epoch and 2022; S—short estimated period covered by nonresolutions; B—no PM anomaly in Brandt (2021); V—artifact caused by telescope vibration. Likely orbital periods P^* are estimated from separation ρ and parallax ϖ as $P^* = (\rho/\varpi)^{3/2} M^{1/2}$, assuming a mass sum of $M = 2\mathcal{M}_\odot$. In the WDS (Mason et al. 2001), these pairs are not removed but are given an X code identifying them as a “dubious double” or a “bogus binary.”

3.4.1. Notes to Individual Spurious Pairs

15073+1827 = A2358AB: this system is another classic “ghost” binary Tokovinin (2012), with many measures and an orbit Eggen (1946), but many unresolved measures and other indications confirming its spurious nature.

18582+1722 = CHR82Aa,Ab: the orbit of Benedict et al. (2007), previously assigned to this pair is obviously the much closer pair CIA14Aa1,2 of Gallenne et al. (2019).

19255+0307 = BNU6Aa,Ab: the ESA (1997) orbit is of the unresolved pair associated with the Kamper et al. (1989) orbit and not the never confirmed wider speckle pair of Bonneau et al. (1980).

4. Summary and Outlook

The program continues to investigate the multiplicity of various stellar samples, the kinematics and dynamics of binary and hierarchical systems, to find new pairs, and to obtain orbital solutions for them as quickly thereafter as possible. Investigation of close pairs have found many that are rapidly moving and others which are anomalous detections and can henceforward be ignored. For those which are rapidly moving, ascertaining the proper observing cadence can be challenging, but we have identified, when possible, specific future instances when observations are needed.

Table 7
Likely Spurious Pairs

WDS	Discoverer	Resolved	Unresolved ^a
00547–2227	B14	0 ^h 1 Vis 1926	2017–19, R
00558–1832	B645	0 ^h 2 Vis 1926	2008–23, R, L, B
01144–0755	WSI70Aa, Ab	0 ^h 2 Sp 2008	2012–21, R, B, V
01380+0946	TOK688	0 ^h 1 Sp 2015	2016–21, R, B, V
01487–3839	I1610AB	0 ^h 3 Vis 1927	2016–22, R, B
04381–1749	B1939	0 ^h 1 Vis 1932	2017–20, R, B
05250–0249	BAG42Aa, Ab	0 ^h 2 Sp 2009	2017–18, R
07074–2127	YSC195	0 ^h 05 Sp 2010	2016–18, R
07346–3336	B1551	0 ^h 2 Vis 1929	2018–19, R, V
08095–4720	WSI55Ba, Bb	0 ^h 1 Sp 2006	2009–2018, V
08246–0109	B527AB	0 ^h 2 Vis 1938	2010–21, R, S
08246–0345	CHR172Aa, Ab	0 ^h 2 Sp 1988	2011–21, R, S, V
10123–3124	WSI128	1 ^h 1 Sp 2010	2015–22, R
11006+0337	CHR33	0 ^h 2 Sp 1983	2014–17, R, B, L
11042–5828	HLN22Aa, Ab	0 ^h 2 Vis 1967	2009, R, L
11317+1422	WSI101Aa, Ab	0 ^h 1 Sp 2001	2011–18, R, S
11479+0815	CHR134Aa, Ab	0 ^h 3 Sp 1987	2014–17, R
11518–0546	CHR36	0 ^h 2 Sp 1983	2014, R, L
11545–5325	YMG39	0 ^h 03 Sp 2019	2019–21, R, S
12062–2002	B1714	0 ^h 1 Vis 1929	2018–22, R, B
12532–0333	CHR38	0 ^h 5 Sp 1984	2013–19, R, S
12543–1139	CHR206	0 ^h 04 Sp 1984	2014–17, R, S
13208–1127	HDS1872	0 ^h 1 HIP	2022, R, L
13212–7427	HDS1874	0 ^h 1 HIP	2021–22, R, B, L
13297–4611	HDS1890	0 ^h 1 HIP	2018, R, B, L
13366–6433	HDS1909	0 ^h 1 HIP	2022, L
13400–7047	HDS1918	0 ^h 1 HIP	2018, R, L
14029–3511	I1574	0 ^h 2 Vis 1927	2017–22, R, B
14141+1258	CHR41	0 ^h 2 Sp 1984	2014, R, B
14157+1911	HDS2003	0 ^h 1 HIP	2019, S
14598–2201	TOK47Aa, Ab	0 ^h 04 Sp 2009	2013–17, R, S
15073+1827	A2358AB	0 ^h 1 Vis 1910	2018–21, R, B, S
15172–3435	BRR10Ba, Bb	0 ^h 7 AO 1994	2022, R, B, L
15210–1522	MCA41	0 ^h 4 Sp 1980	2008–14, R, L
15355–1447	WRH20Aa, Ab	0 ^h 1 Vis 1937	2009–23, S
15462–2804	CHR50Aa, Ab	0 ^h 2 Sp 1983	2009–22, S
16102–4008	I1082AB	0 ^h 4 Vis 1912	2008–22, R, B, L
16133+1332	CHR52Aa, Ab	0 ^h 2 Sp 1983	2008–09, R, S
16142–5047	TOK409	0 ^h 1 Sp 2014	2015–22, R, B, S, V
16406+0413	CHR56Aa, Ab	0 ^h 1 Sp 1985	2014–22, R, B, V
16438–5330	CHR147Aa, Ab	0 ^h 04 Sp 1989	2008–14
16542–4150	CHR252Aa, Ab	0 ^h 1 Sp 1994	2009–19, R, L
16593–1926	HDS2403	0 ^h 4 HIP	2018, L, R
17376–1524	ISO6Aa, Ab	0 ^h 3 Sp 1987	2023, B
17449–5733	HLN44Aa, Ab	0 ^h 2 Vis 1967	2008–19, R, B
18073+0934	STT342Aa, Ab	1 ^h 3 Vis 1842	2023, B
18218–1619	CHR69	0 ^h 1 Sp 1985	2013–18, R, L
18237+2146	TOK60Aa, Ab	0 ^h 04 Sp 2009	2018–21, B, V, L
18367+0640	CHR76Aa, Ab	0 ^h 1 Sp 1985	2008–09, R, B, S
18448–2501	CHR78	0 ^h 1 Sp 1983	2014–19, R, V
18582+1722	CHR82Aa, Ab	0 ^h 2 Sp 1984	2015, R, L
19098–2101	FIN311AB	0 ^h 1 Vis 1936	2009–18
19098–2101	FIN311AC	0 ^h 4 Vis 1936	2009–18
19247+0833	WSI108	0 ^h 1 Sp 2008	2015–21, R, B, S
19255+0307	BNU6Aa, Ab	0 ^h 1 Sp 1979	2023, S
19298–1102	HDS2771	0 ^h 1 HIP	2015–21, R, B
19409–0152	TOK424	0 ^h 04 Sp 2014	2015–21
20011+0931	CHR118	0 ^h 2 Sp 1985	2018, R, L

Note.

^a Additional indications of the spurious nature of resolutions: R—no excess noise in Gaia DR3, $\text{RUWE} < 2$; L—long estimated period; B—no significant PM anomaly in (Brandt 2021); S—short estimated period or spectroscopic coverage; V—artifact caused by SOAR vibration.





Acknowledgments

We thank the SOAR operators for efficient support of this program and the SOAR director J. Elias for allocating some technical time. This work is based in part on observations carried out under CNTAC programs CN2019A-2, CN2019B-13, CN2020A-19, CN2020B-10, and CN2021B-17. R.A.M. and E.C. acknowledge support from the FONDECYT/CONICYT grant #1190038. The research of A.T. is supported by the NSF's NOIRLab.

This work used the SIMBAD service operated by Centre des Données Stellaires (Strasbourg, France), bibliographic references from the Astrophysics Data System maintained by SAO/NASA and the Washington Double Star Catalog maintained at the USNO. This work has made use of data from the European Space Agency (ESA) mission Gaia (<https://www.cosmos.esa.int/gaia>) processed by the Gaia Data Processing and Analysis Consortium (DPAC; <https://www.cosmos.esa.int/web/gaia/dpac/consortium>). Funding for the DPAC has been provided by national institutions, in particular the institutions participating in the Gaia Multilateral Agreement.

Facility: SOAR.

ORCID iDs

Brian D. Mason  <https://orcid.org/0000-0003-4824-0938>
 Andrei Tokovinin  <https://orcid.org/0000-0002-2084-0782>
 Rene A. Mendez  <https://orcid.org/0000-0003-1454-0596>
 Edgardo Costa  <https://orcid.org/0000-0003-4142-1082>

References

- Aitken, R. G. 1964, *The Binary Stars* (New York: Dover), 110
- Anguita-Aguero, J., Mendez, R., Clavería, R. M., & Costa, E. 2022, *AJ*, 163, 118
- Batten, A. H., Fletcher, J. M., Hill, G., Wenxian, L., & Morbey, C. L. 1991, *PASP*, 103, 294
- Benedict, G. F., McArthur, B. E., Feast, M. W., et al. 2007, *AJ*, 133, 1810
- Bonneau, D., Blazit, A., Foy, R., & Labeyrie, A. 1980, *A&AS*, 42, 185
- Brandt, T. D. 2021, *ApJS*, 254, 42
- Duquennoy, A., Mayor, M., & Halbwachs, J.-L. 1991, *A&AS*, 88, 281
- Eggen, O. J. 1946, *AJ*, 52, 81
- ESA 1997, ESA SP-1200, *The Hipparcos and Tycho Catalogues* (Noordwijk: ESA)
- Gaia Collaboration, et al. 2018, *A&A*, 616A, 1
- Gaia Collaboration, Brown, A. G. A., Vallenari, A., et al. 2021, *A&A*, 649, A1
- Gallenne, A., Kervella, P., Borgniet, S., et al. 2019, *A&A*, 622A, 164
- Gómez, J., Docobo, J. A., Campo, P., et al. 2022, *MNRAS*, 509, 4229
- Harris, D. L., III, Strand, K. A., & Worley, C. E. 1963, in *Stars and Stellar Systems*, Vol. 3, Basic Astronomical Data, ed. K. A. Strand (Chicago, IL: Univ. Chicago Press), 273
- Hartkopf, W. I., Mason, B. D., & Worley, C. E. 2001, *AJ*, 122, 3472
- Hartkopf, W. I., McAlister, H. A., & Franz, O. G. 1989, *AJ*, 98, 1014
- Hartkopf, W. I., Tokovinin, A., & Mason, B. D. 2012, *AJ*, 143, 42
- Horch, E. I., Tokovinin, A., Weiss, S. A., et al. 2019, *AJ*, 157, 56
- Horch, E. P., Broderick, K. G., Casetti-Dinescu, D. I., et al. 2021, *AJ*, 161, 295
- Horch, E. P., Casetti-Dinescu, D. I., Amarata, M. A., et al. 2017, *AJ*, 153, 212
- Horch, E. P., van Belle, G. T., Davidson, J. W., Jr, et al. 2015, *AJ*, 150, 151
- Izmailov, I. S. 2019, *AstL*, 45, 30
- Kamper, K. W., Legget, D., & McCarthy, D. W. 1989, *AJ*, 98, 686
- Mann, A. W., Dupuy, T., Kraus, A., et al. 2019, *ApJ*, 871, 63
- Mason, B. D., Wycoff, G. L., Hartkopf, W. I., et al. 2001, *AJ*, 122, 3466
- McAlister, H. A., Mason, B. D., Hartkopf, W. I., & Shara, M. M. 1993, *AJ*, 106, 1639
- Mendez, R. A., Clavería, R. M., & Costa, E. 2021, *AJ*, 161, 155
- Mendez, R. A., Clavería, R. M., Orchard, M. E., & Silva, J. F. 2017, *AJ*, 154, 187
- Tokovinin, A. 2012, *AJ*, 144, 56
- Tokovinin, A. 2016a, *AJ*, 152, 138
- Tokovinin, A. 2016b, *Orbit: IDL Software For Visual, Spectroscopic, And Combined Orbits*, Zenodo, doi:10.5281/zenodo.61119
- Tokovinin, A. 2017, *AJ*, 154, 110
- Tokovinin, A. 2018, *PASP*, 130, 035002
- Tokovinin, A. 2021a, *AJ*, 161, 144
- Tokovinin, A. 2021b, *Univ*, 7, 352
- Tokovinin, A. 2023, *AJ*, 165, 180
- Tokovinin, A. 2023, *AJ*, 165, 165
- Tokovinin, A., & Latham, D. W. 2020, *AJ*, 160, 251
- Tokovinin, A., Mason, B. D., & Hartkopf, W. I. 2010a, *AJ*, 139, 743
- Tokovinin, A., Cantarutti, R., Tighe, R., et al. 2010b, *PASP*, 122, 1483
- Tokovinin, A., Mason, B. D., & Hartkopf, W. I. 2014, *AJ*, 147, 123
- Tokovinin, A., Mason, B. D., Hartkopf, W. I., et al. 2015, *AJ*, 150, 50
- Tokovinin, A., Mason, B. D., Hartkopf, W. I., et al. 2016, *AJ*, 152, 116
- Tokovinin, A., Mason, B. D., Hartkopf, W. I., et al. 2018, *AJ*, 155, 235
- Tokovinin, A., Mason, B. D., Mendez, R. A., et al. 2019, *AJ*, 158, 48
- Tokovinin, A., Mason, B. D., Mendez, R. A., et al. 2020, *AJ*, 160, 7
- Tokovinin, A., Mason, B. D., Mendez, R. A., et al. 2021, *AJ*, 162, 41
- Tokovinin, A., Mason, B. D., Mendez, R. A., & Costa, E. 2022, *AJ*, 164, 58
- van Leeuwen, F. 2007, *A&A*, 474, 653
- Vrijmoet, E. H., Tokovinin, A., Henry, T. J., et al. 2022, *AJ*, 163, 178
- Worley, C. E., & Behall, A. L. 1973, *AJ*, 78, 650
- Ziegler, C., Tokovinin, A., Briceño, C., et al. 2020, *AJ*, 159, 19
- Ziegler, C., Tokovinin, A., Latiolais, M., et al. 2021, *AJ*, 162, 192